Karazin Kharkiv National University
Department of Physics and Technology

Technische Universität Darmstadt
Institut für Kernphysik

Feasibility Study of K-Ar Dating using the $^{39}K(\gamma, n)$ Reaction at the S-DALINAC

Diploma Thesis

Olena Yevetska

Darmstadt

February 2003

Contents

Abstract

In this diploma thesis an investigation of the feasibility of $^{39}K(\gamma, n)$ experiments at the S-DALINAC for determination of the age of minerals is presented. The geometry and results of numerous simulations for qualitative and quantitative predictions of ^{38}Ar production from the $^{39}K(\gamma, n)$ reaction are given. The fully integrated particle physics Monte Carlo package FLUKA was used for the simulations.

The simulation results permit an optimization of the experimental parameters because accurate predictions for the importance of the photo-induced reactions interfering with the production of ^{38}Ar can be made. The accuracy of qualitative predictions is tested and compared to the results of a prototype experiment performed at the AERE, Harwell, accelerator. The beam time for a probe irradiation is estimated .

A possible experimental setup for carrying out according experiments at the superconducting Darmstadt electron linear accelerator S-DALINAC is described.

AbstractR

i

1 Introduction

Potassium is one of the most abundant elements in nature and is present in sedimentary rocks. The existence of the primordial radioactive isotope ^{40}K allows geological age dating due to the decay of naturally occuring ^{40}K to stable ^{40}Ar. Most of the literature on argon isotopes [1, 2] deals with the measurement of ^{40}Ar dating the age of rocks using so-called K-Ar technique. The conventional K-Ar method of dating depends on the assumption that the sample contained no argon at the time of its formation and that subsequently all radiogenic argon produced inside it was quantitatively retained [1]. Minerals are dated by the measurement of the concentration of ^{40}K and the amount of radiogenic ^{40}Ar that has been accumulated.

Argon is a noble gas. The main isotopes of argon in terrestrial systems are ^{40}Ar (99.600%), ^{36}Ar (0.337%), and ^{38}Ar (0.063%). The isotope ^{40}K has a half-life of $1.277 \cdot 10^9$ years. The naturally occurring ^{40}K decays to the stable ^{40}Ar (10.679%) via electron capture and positron emission, and decays to the stable ^{40}Ca (89.280%) via β^--decay [3]. The decay scheme diagram is shown in Fig. 1.

As mentioned above, ^{40}K is widely distributed in nature and is present in minerals that were formed in all geological environments - volcanic, sedimentary etc. and this fact constitutes the main advantage of this method. But the requirements for a successful K-Ar dating may under certain conditions be violated. Because argon may be lost by diffusion even at temperatures well below the melting point, K-Ar dates may, instead of the real age, represent the time elapsed since the sample has cooled down to the certain

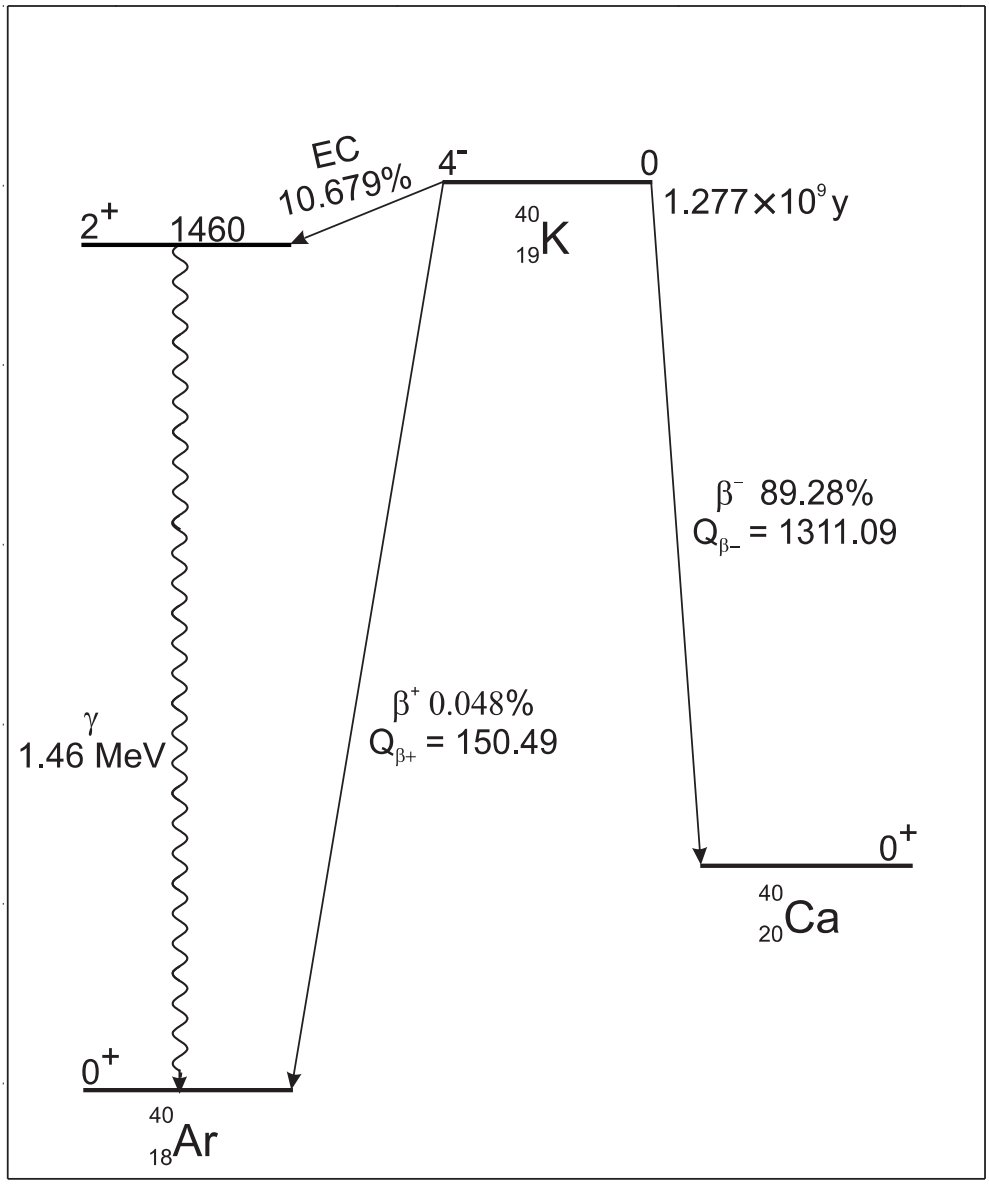

Figure 1: Decay scheme diagram for the branched decay of ^{40}K to ^{40}Ar via electron capture and positron emission and to ^{40}Ca via emission of negative electrons [3].

temperatures at which diffusion loss of argon is insignificant, thus leading to an underestimation of the age. Under certain circumstances an excess of radiogenic ^{40}Ar might occur which would cause K-Ar dates to overestimate the age. For example, when rock or lava cools down to a solid state from a molten one it becomes, apart from the surface, essentially impermeable to gases and any argon generated subsequently is retained in the rock, trapped in the crystal lattice. What is measured as the "age" of the rock then is the length of time that had passed since it was molten.

The $^{40}Ar/^{39}Ar$ method of dating can overcome some of the limitations of the conventional K-Ar method. This method of argon-argon dating [1, 4, 5] is based on the formation of ^{39}Ar as a result of the irradiation of K-bearing samples with fast neutrons (typical through the $^{39}K(n,p)$ reaction) using it as an indirect measure of the potassium content of a mineral. The method has the additional advantage that potassium and argon are determined on the same sample and that only measurements of the isotopic ratios of argon are required. The problem of inhomogeneity of samples and the need to measure the absolute concentrations of potassium and argon are thus eliminated. It is suitable even for small and precious samples.

But a number of workers have pointed out the existence of interfering reactions in the method [6, 7] and proposed elaborate procedures for correcting for produced "interfering isotopes", either by optimizing the irradiation parameters, or by the use of argon isotopic ratios measured in irradiated standard minerals. The source of this difficulty lies in the fact that the threshold energies of the neutron induced reactions are low compared with the energy of the fast neutrons required to generate ^{39}Ar from the $^{39}K(n,p)$ reaction [8].

The maximum cross section for this reaction occurs for neutrons with energy 3 MeV. Another problem are probes with small grain size. There, the recoil momentum of the produced ^{39}Ar can be large enough to expel the produced atom which then is lost because of its gaseous nature.

Thus, alternative methods, in particular to avoid the latter problem, are of high interest. One possibility is the $^{39}K(\gamma, n)$ reaction. The feasibility of such an experiment has been demonstrated in a prototype experiment [9]. This experiment is described below in Chapter 4.1. The purpose of the present diploma thesis is to investigate the feasibility of such experiments using the high-energy photon production setup existing at the S-DALINAC.

This thesis is divided into six chapters. The theoretical aspects are presented in the Chapter 2. Chapter 3 focuses on the description of the FLUKA code and it represents the results of simulation. The problem of the interfering reactions is discussed in Chapter 4. Chapter 5 covers details of the possible experiment at the S-DALINAC. The conclusion is given in Chapter 6.

2 Theoretical Aspects

2.1 The $^{38}Ar/^{40}Ar$ Method

The reaction under investigation is

$$^{39}K(\gamma, n)^{38}K \xrightarrow{\beta^+} {}^{38}Ar, \tag{1}$$

in which ^{38}K produced from ^{39}K in a photoneutron reaction subsequently decays to ^{38}Ar via β^+ emission with a half - life of 7.7 min, and all ^{38}Ar is available for a measurement within a few hours after the irradiation. The threshold energy for the reaction is 13.1 MeV [10] and a resonant peak in the photon absorption spectrum shown in Fig. 2 occurs at about 21 MeV with a cross section of 25 mb. If one subtracts the (γ, np) partial cross section indicated by the dashed line in Fig. 2 from the total representing the sum of the $^{39}K(\gamma, n)$ and (γ, np) reactions, a negligible cross section above around 25 MeV is found [11].

Thus, if a mineral sample of age t is irradiated with photons of energy in excess of 13 MeV to determine age with the help of argon - argon method, in the absence of interfering reactions that produce ^{38}Ar, too, it will contain after the irradiation [8] the amount of the photon-induced ^{38}Ar

$$N(^{38}Ar) = N(^{39}K)\Delta T \int \phi(E)\sigma(E)dE, \tag{2}$$

with $N(^{39}\mathrm{K})$ - the number of atoms of ^{39}K present in sample,

$N(^{38}\mathrm{Ar})$ - the number of ^{38}Ar atoms produced by irradiation,

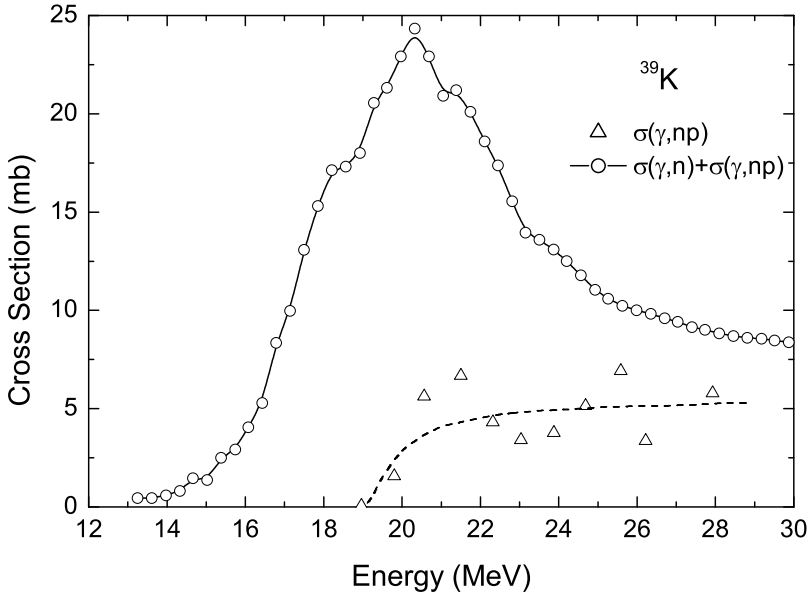

Figure 2: Partial photoneutron cross sections [11] for ^{39}K. The full line connects experimental points for the sum of the $^{39}K(\gamma, n)$ and (γ, np) reactions. The dashed line presents a fit to values of the (γ, np) reaction.

$\phi(E)$ - the photon flux at energy E,

$\sigma(E)$ - the cross section of $^{39}K(\gamma, n)^{38}K$ reaction at energy E,

ΔT - the duration of the sample irradiation.

The integration is performed over all incident photon energies.

On the other hand the amount of the radiogenic ^{40}Ar is given by

$$N(^{40}Ar^*) = \frac{\lambda_e}{\lambda_e + \lambda_\beta} N(^{40}K)(e^{t/\tau} - 1), \tag{3}$$

with $N(^{40}\mathrm{K})$ - the number of $^{40}\mathrm{K}$ atoms present in a sample,

$N(^{40}\mathrm{Ar}^*)$ - the number of radiogenic argon in a sample,

$\lambda_e = 0.584 \times 10^{-10}\ yr^{-1}$ - the decay constant of $^{40}\mathrm{K}$ by K-electrons capture,

$\lambda_\beta = 4.72 \times 10^{-10}\ yr^{-1}$ - the decay constant of $^{40}\mathrm{K}$ by β-emission,

τ - the mean life of $^{40}\mathrm{K}$, given by

$$\tau = (\lambda_e + \lambda_\beta)^{-1}. \tag{4}$$

From Eqs. (3) and (2) one can deduce the ratio

$$\frac{N(^{40}Ar^*)}{N(^{38}Ar)} = \frac{N(^{40}K)}{N(^{39}K)} \frac{\lambda_e}{\lambda_e + \lambda_\beta} \frac{1}{\Delta T} \frac{(e^{t/\tau} - 1)}{\int \phi(E)\sigma(E)dE}. \tag{5}$$

As for the $^{40}\mathrm{Ar}/^{39}\mathrm{Ar}$ dating method one defines an irradiation parameter J

$$J = \frac{N(^{39}K)}{N(^{40}K)} \frac{\lambda_e + \lambda_\beta}{\lambda_e} \Delta T \int \phi(E)\sigma(E)dE, \tag{6}$$

and according to Eq. (5) it follows that

$$J = \frac{e^{t/\tau} - 1}{N(^{40}Ar^*)/N(^{38}Ar)} = \frac{Q}{N(^{40}Ar^*)/N(^{38}Ar)}, \tag{7}$$

where

$$Q = e^{t/\tau} - 1. \tag{8}$$

From Eq. (7), J can be identified as being a function of the ratio $^{40}\mathrm{Ar}^*/^{38}\mathrm{Ar}$ in a particular irradiated sample and its age t which can be deduced from the potassium decay.

In order to test the possibility of measuring isotopic ages using this procedure it is necessary to irradiate a number of samples of known potassium-argon ages, inserted into a sample holder at known positions between the samples of unknown age, in the same photon flux and to determine the value of J for each of them using Eq. (7). Then the J values are plotted as a function of the position in the sample holder. The respective J values of the unknown samples are obtained by interpolation of the resulting graph from their known positions in the holder. The $^{40}Ar^*/^{38}Ar$ ratios of the unknown samples are then used to calculate the age from

$$t = \tau \ln(\frac{^{40}Ar^*}{^{38}Ar} J + 1). \tag{9}$$

Several different mineral concentrates have been employed as flux monitors. Their ages must be accurately known because they are used for calculation of the value J in the Eq. (7). An error in the age of the monitor propagates therefore from Eq. (7) to Eq. (9) and results in a corresponding systematic error in the calculated $^{40}Ar/^{38}Ar$ dates of the samples that were irradiated together with that monitor.

Having determined from Eq. (7) the J value for the sample of a "known" age and knowing the ratio of $^{40}Ar/^{38}Ar$ in the sample under investigation one can thus obtain its age using Eq. (9).

2.2 Bremsstrahlung: some Features

The most intense photon source available in the MeV range is bremsstrahlung. Therefore, one must know how the photon spectrum re-

sulting from the conversion of an electron beam into bremsstrahlung looks like.

When a swiftly moving charged particle of mass m and charge z passes close to a nucleus of charge Z, it experiences a Coulomb force proportional to $z \cdot Z$ and consequently undergoes an acceleration proportional to $z \cdot Z/m$. According to classical physics, an accelerated charge radiates electromagnetic energy at a rate proportional to $z^2 \cdot Z^2/m^2$. The proportionality to the square of the atomic number means that the energy losses by radiation should be much more important in heavy elements than in light ones, while the inverse proportionality to the square of mass implies that light particles should radiate much more readily than the heavy ones. Consequently, radiation as an energy loss mechanism is usually significant for electrons only. It is called bremsstrahlung.

The bremsstrahlung energy spectrum extends from zero to the energy of the initial electrons. The classical representation of the bremsstrahlung process for electrons is as follows: an electron of the energy E_0, moving in the Coulomb field of the nucleus, can change its direction of motion. However, since every change of the direction involves an acceleration, then according to classical concepts of charge acceleration, it is probable that while in passing a nucleus the electron will emit a quantum of energy E_γ and will drop to a new state of the energy E. But since the nucleus in which field the photon is emitted is considerably heavier than the electron, it can acquire, in principle, any momentum transfer. As a consequence there is a probability that after emitting a photon the electron can drop to any final state of the energy E, as long as the law of energy conservation is conserved. In other words, the

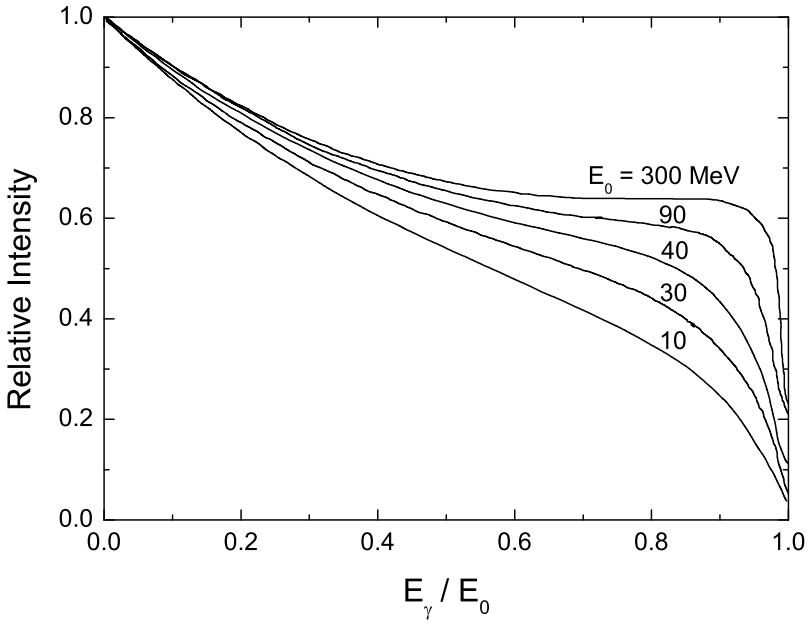

Figure 3: Bremsstrahlung spectrum [12] for electrons of various energies on platinum (Z=78), normalized to unity at $E_\gamma = 0$.

bremsstrahlung spectrum should be continuous over the range of photon energies from 0 to $E_0 - m_0c^2$ where m_0 and c are the rest mass of the electron and the speed of light, respectively [12]. Typical distributions for a number of electron energies on platinum (Z=78) are shown in Fig. 3.

The average opening angle $\bar{\theta}$ of the emission cone of bremsstrahlung photons at relativistic energies is given approximately by the well-known formula

$$\bar{\theta} \approx \frac{mc^2}{E_0} . \tag{10}$$

After the quantum is emitted, the electron continues to move under a finite

angle with respect to the initial direction.

As pointed out above, the rate of the energy loss by radiation is roughly proportional to the square of the atomic number of the stopping material. It also increases rapidly with energy, being negligible below 100 keV and rising to values greater than the rate of energy loss by collisions at energies between 10 and 100 MeV, depending on the material. In the relativistic limit $E_0 \gg 137mc^2Z^{-1/3}$, where the screening of the nuclear charge by the atomic electrons is complete, the rate of the energy loss is given by [13]

$$-\left(\frac{dE}{dx}\right)_{rad} = 4Z(Z+1)r_0^2 n\alpha E_0 \ln(183Z^{-1/3}), \tag{11}$$

where n is the number of target atoms per cm^3, α is the fine structure constant and r_0 is the classical electron radius.

The energy E_c, at which the losses due to collisions and bremsstrahlung for electrons are the same, that is

$$\left(\frac{dE_c}{dx}\right)_{rad} = \left(\frac{dE_c}{dx}\right)_{coll}, \tag{12}$$

is called "critical energy". Above this energy the radiation loss will dominate over the collision-ionization losses. An approximate formula for E_c is given by [14]

$$E_c = \frac{800}{Z+1.24}\,[MeV]\,. \tag{13}$$

The ratio of the radiation loss to the collision loss at the energy E_c is approximately

$$\frac{(dE/dx)_{rad}}{(dE/dx)_{coll}} \approx \frac{E_0 \cdot Z}{1600 \cdot mc^2}\quad . \tag{14}$$

It can be seen from Eq. (14) that in graphite (Z=6) the radiation loss becomes

comparable to the collision loss only at energies above 100 MeV, while in lead (Z=82) these two are equal already at about 10 MeV.

Above the critical energy the electrons will lose their energy according to

$$E = E_0 \cdot \exp\left(-\frac{L}{L_{rad}}\right), \tag{15}$$

where L is the travelled distance and L_{rad} is the radiation length. For quick calculations, the following convenient expression for L_{rad} can be used [15]

$$L_{rad} = \frac{716.4 \cdot A}{Z(Z+1)\ln\left(287/\sqrt{Z}\right)} \left[\frac{g}{cm^2}\right], \tag{16}$$

where A is the mass number of the target.

Using the atomic model of Thomas and Fermi, Schiff [16] obtained the following expression for the bremsstrahlung cross section for full screening and relativistic energies of the incident electrons

$$\begin{aligned}\sigma_\gamma(E_\gamma,\theta)dE_\gamma d\theta = {} & \tfrac{8Z(Z+1)r_0^2}{137} \cdot \tfrac{dE_\gamma}{E_\gamma} \cdot \tfrac{E_0-E_\gamma}{E_0} \cdot \tfrac{xdx}{1+x^2} \cdot \\ & \left\{\left[\tfrac{E_0}{E_0-E_\gamma} + \tfrac{E_0-E_\gamma}{E_0} - \tfrac{4x^2}{(1+x^2)^2}\right] \cdot \ln\left(\tfrac{2E_0(E_0-E_\gamma)}{mc^2E_\gamma}\right) - \right. \\ & \left. -\tfrac{1}{2}\left[\tfrac{E_0}{E_0-E_\gamma} + \tfrac{E_0-E_\gamma}{E_0} + 2 - \tfrac{16x^2}{(1+x^2)^2}\right]\right\}.\end{aligned} \tag{17}$$

Here, $x = \frac{E_0}{mc^2} \cdot \theta$ is the reduced photon emission angle. Note, however, that Eq. (17) is accurate for infinitely thin targets only.

2.3 FLUKA: Modeling Photon Spectra

Atomic scattering in the radiator changes the trajectory of the electrons. As discussed above, the resulting bremsstrahlung depends on the initial energy E_0 and the angle θ. Therefore, the interplay of those processes needs to be

taken into account which can only be realized using Monte Carlo techniques. Furthermore, in Monte Carlo codes one can implement a realistic geometry of the probe in order to obtain the impinging photon spectrum. One example of such a code is FLUKA [17].

FLUKA is a fully integrated particle physics Monte-Carlo simulation package. This code originated from J. Ranft (CERN) at the beginning of the seventies for simulating particle cascades (FLUKA is the abbreviation formed from the German expression "Fluktuierende Kaskade"). It has found many applications in high energy experimental physics and engineering, shielding, detector and telescope design, cosmic ray studies, dosimetry, medical physics and radiobiology.

FLUKA calculates the transport and interaction of electrons, positrons and photons by the Monte-Carlo method. The geometry, materials and their properties, possible electric and magnetic fields are defined in an input file. The simulation geometry is surrounded by a sufficiently large, all-absorbing region, the so-called "black hole", which has an infinite absorption cross-section, and all particles vanish when they reach it. Also, the primary particles properties are determined: particle type and energy, geometry and position of the beam and the number of primary particles used.

During the simulation FLUKA tracks the further evolution of each primary particle. At the time of interaction with the mentioned materials, primary particles could be scattered elastically or inelastically or decay to other particles. It is possible to follow the secondary particles, emergent as a result e.g. of electromagnetic cascades. The particle tracking is stopped when

- the particle energy decreases below a predefined energy minimum, when the energy of the charged particles drops below the cut-off, the particles are not stopped, but are transported in straight lines until they come to rest;

- the particle leaves the simulation volume and is absorbed by a "black hole" region.

When all particles in the electromagnetic cascade induced by the primary particle were counted, FLUKA begins the simulation for the next one. At the time of simulation it is possible to register events, that were prescribed before, as for example, particle passage from one part of the volume to another one etc. At the end of the simulation FLUKA gives out the so-called "boundary-crossing flow" N_γ as a function of energy and solid angle, divided into predefined bins. This quantity is determined as

$$N_\gamma = \frac{N}{N_p \Delta E \Delta\Omega A_{\mathrm{det}}} \ , \tag{18}$$

with N - amount of particles of certain kind that passed the corresponding boundary in a certain direction,

N_p - amount of primary particles,

ΔE - energy bin width,

$\Delta\Omega$ - solid angle bin width,

A_{det} - effective surface of the detector.

The values of ΔE and A_{det} are assigned in the input file. The solid angle value in the direction between incoming and outcoming particles is equal to the half of the full solid angle, i.e. 2π.

2.4 Photoneutron Reactions

If a nucleus is bombarded with photons of energies above the particle thresholds, it can absorb these γ - quanta and emit protons, neutrons and other particles. Such processes are called photonuclear reactions. The reactions (γ, n) and (γ, p) have been studied most of all. Depending on the mass number A, in the energy region of 10 - 25 MeV the photonuclear cross section has a broad maximum with the width of 3 - 5 MeV [18], the so-called giant dipole resonance. It occurs in almost all nuclei except for the lightest ones [19, 20]. It corresponds to the fundamental frequency for absorption of electric dipole radiation by the nucleus acting as a whole, and is most simply understood as the counter - oscillation of neutrons and protons with respect to each other in the nucleus.

In Fig. 4 the general shape of the photoneutron-production cross sections for a heavy nuclide ($A > 60$), where neutron emission dominates, is shown. The giant dipole resonance rising to values around of 100 millibarns occurs several MeV above the (γ, n) threshold. The total photonuclear cross section falls off abruptly above the giant dipole resonance and then, according to [21] rises slowly up to about half the resonance peak at 320 MeV. The GDR peak is well approached by a Lorentz curve in spherical nuclei or a superposition of two Lorentz curves in deformed ones.

The peak energy E_m has been predicted by collective models of the GDR to be proportional either $A^{-1/3}$ or $A^{-1/6}$ [19]. The $A^{-1/3}$ dependence arises from the concept that when displacement of the neutron and proton fluids occurs, the restoring force is proportional to the density gradient of those fluids [22].

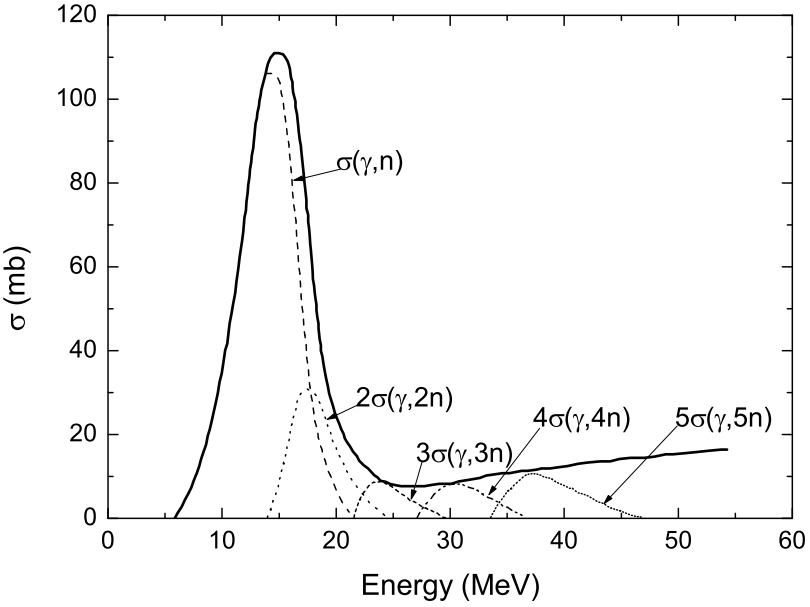

Figure 4: Schematic illustration of photoneutron-production cross section, showing qualitatively the contribution of (γ,n), (γ,2n),(γ,3n),(γ,4n) and (γ,5n) processes [18].

The $A^{-1/6}$ dependence of E_m is based on the concept that the restoring force is proportional to the nuclear surface area [22, 23]. Experimentally, one finds that a combination $E_m \sim A^{-1/3} + A^{-1/6}$ gives the best fit.

The $(\gamma, 2n)$, $(\gamma, 3n)$,... processes make appreciable contributions to the photoneutron - production cross section above the corresponding thresholds. If one assumes that, because of the Coulomb barrier, the cross sections for the production of charged particles are much smaller than the cross sections for neutron production, then one may interpret the curve shown in Fig. 4 as

the photon-capture cross section multiplied by the average number of neutrons emitted per event. These processes are unwanted for the application discussed here and set an upper limit for the useful photon energy range.

3 FLUKA Simulations

3.1 Geometry and Parameters

The geometry selected for the simulations of the present problem is shown in Fig. 5, where ① denotes the probe, ② is the gold target (radiator) and ③ is the "black hole" region.

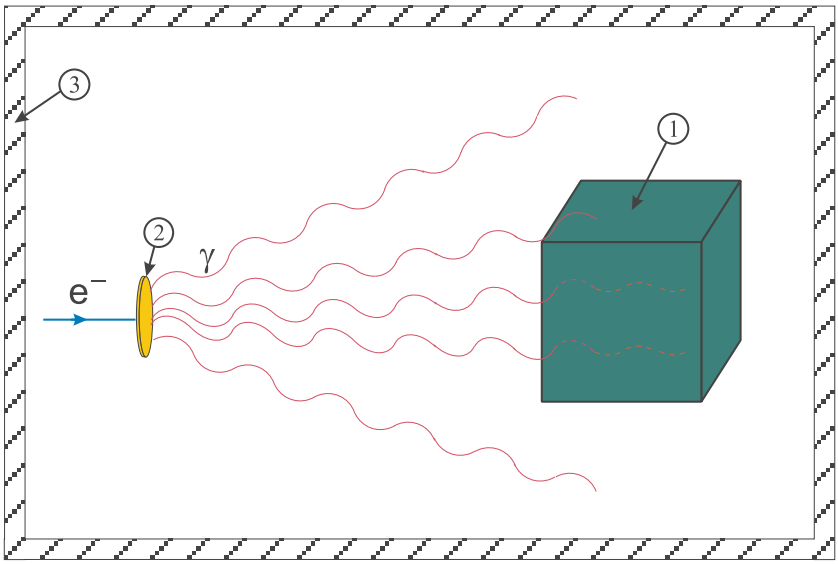

Figure 5: Simulation geometry (schematic). ① - probe, ② - gold target, ③ - "black hole".

The probe ① consists of potassium and is irradiated by a continuous bremsstrahlung pencil-beam, which is produced by decelerating electrons in a conversion target ② , called radiator. The electron energies used for the simulation are 20, 25, 30 and 35 MeV. These values were chosen because the thresholds of $^{39}K(\gamma, n)$ and $^{40}Ca(\gamma, np)$ reactions lie in this region. The

radiator is a disk with a radius of 0.1 cm and a thickness of $t = 0.033$ cm which corresponds to 10% of the radiation length of gold. These parameters are determined by the existing experimental setup.

The probe is a cube with a side length of 1 cm. The distance between the radiator and the probe is 15 cm. This value is due to the experimental setup, too. The number of test particles is 10^7 determined by the typical length of time for a run of about 2 days.

3.2 Results

FLUKA allows to obtain the photon angular and energy distributions.

The number of energy bins can be set in the program. In our simulation 100 bins were chosen for the energy distribution and 1000 bins for the angular one. Examples of energy and angular distributions for the 25 MeV electron beam are shown in Figs. 6 and 7, respectively. The energy distribution allows us to calculate the production rate of ^{38}Ar atoms [see Fig. 9]. From the angular distribution one can obtain the angle spreading for different beam energies after passing through the radiator material (see Table 1).

The results for N_γ are always given as double differential distributions of the flow [see Eq. (18)] per energy and solid angle (cm^{-2}, GeV^{-1}, sr^{-1} per incident primary unit weight), even when only 1 interval (bin) has been requested. Thus one must multiply each output value for normalization by the factor $A_{\rm det}E_o\Omega Pn^{-1}$, where A_{det} is the effective surface of the detector (in cm^2), E_0 is the electron beam energy (in GeV), Ω is equal to 2π or 4π (depending on whether one-way or two-way scoring has been requested), P is the number

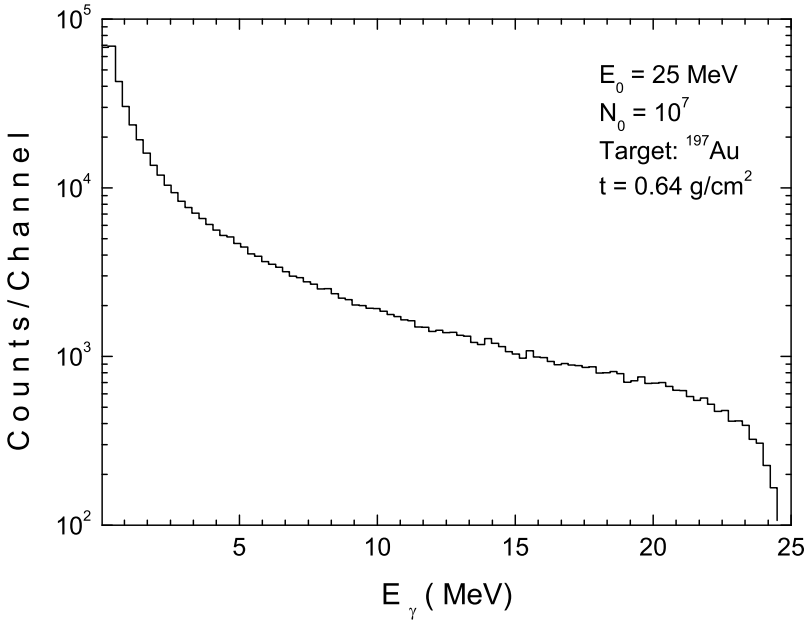

Figure 6: Example of the photon energy distribution obtained by means of a FLUKA simulation.

of primary particles and n is the number of bins.

The ^{38}Ar amount produced in the probe can be obtained from the following expression

$$N(^{38}Ar) = t\frac{N_A}{A}\rho\sum\sigma N_\gamma, \tag{19}$$

where t is the probe thickness, N_A is Avogadro's number, ρ is the potassium density, σ is the photoneutron cross section and N_γ is the flux of photons.

The amount of ^{38}Ar atoms induced in the sample is given in Table 1 for different electron energies. The calculations were made for a beam current of $10\mu A$. The incident electron energy dependence of the ^{38}Ar amount is shown

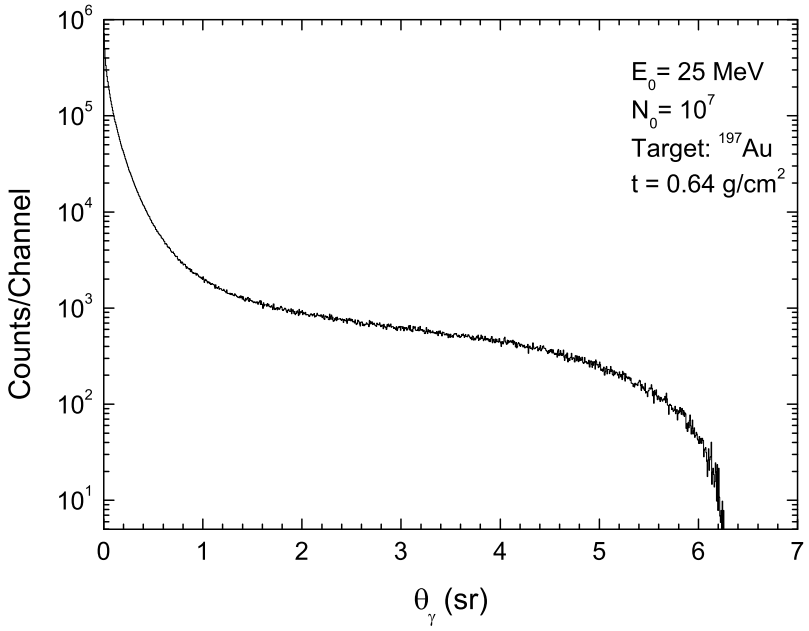

Figure 7: Example of the photon angular distribution obtained by means of a FLUKA simulation.

in the upper part of Fig. 8. It becomes apparent that a quadratic function $Y = B_0 + B_1X + B_2X^2$ provides a good approximation and can be used for further interpolation. The parameters $B_0 = -4.055$, $B_1 = 0.0687$ and $B_2 = 0.0085$ were used to produce the curve shown.

Also, the results for the most important interfering reaction $^{40}Ca(\gamma, np)$, discussed later in Chapter 4.3, are shown. The fit function is also quadratic with parameters $B_0 = 3.486$, $B_1 = -0.296$ and $B_2 = 0.00628$.

Figure 9 displays the results of σN_γ (production) for the simulation with a 30 MeV electron beam. The upper part represents the value of N_γ, the mid-

Table 1: Yield Comparison for different Energies.

Energy	σN_γ	Angular Spreading		^{38}Ar Amount
(MeV)	(mb/s)	(sr)	(degree)	(atoms/s)
20	73733	0.0648	1.86	6.18×10^6
25	333850	0.2265	0.65	2.07×10^7
30	564465	0.0192	0.55	4.85×10^7
35	843860	0.01424	0.41	7.35×10^7

dle part shows the photoneutron cross section for $^{39}K(\gamma, n)$ reaction which was obtained by substracting the (γ, np) partial cross section from the total representing the sum of the $^{39}K(\gamma, n)$ and (γ, np) reactions, and the bottom part displays the production value. The fluctuations in the photon spectra are due to the limited statistics by using only 10^7 incident particles in the FLUKA simulation. As one can see, despite the strong energy dependence of the photon spectrum, the energy dependence of the production rate is determined largely by the behavior of $\sigma(E_\gamma)$.

3.3 Discussion

As it was calculated before [24] we should have 10^{13} atoms of ^{38}Ar from 1 g of ^{38}K for an experiment. Under existing conditions (e. g. beam current $10\mu A$) from Table 1 one can estimate that 5 days for the irradiation are necessary at a beam energy of 25 MeV, 2 days at 30 MeV and approximately 36 hours at 35 MeV. But using the 35 MeV electron beam one has a problem of the interfering reactions [see Chapter 4.3].

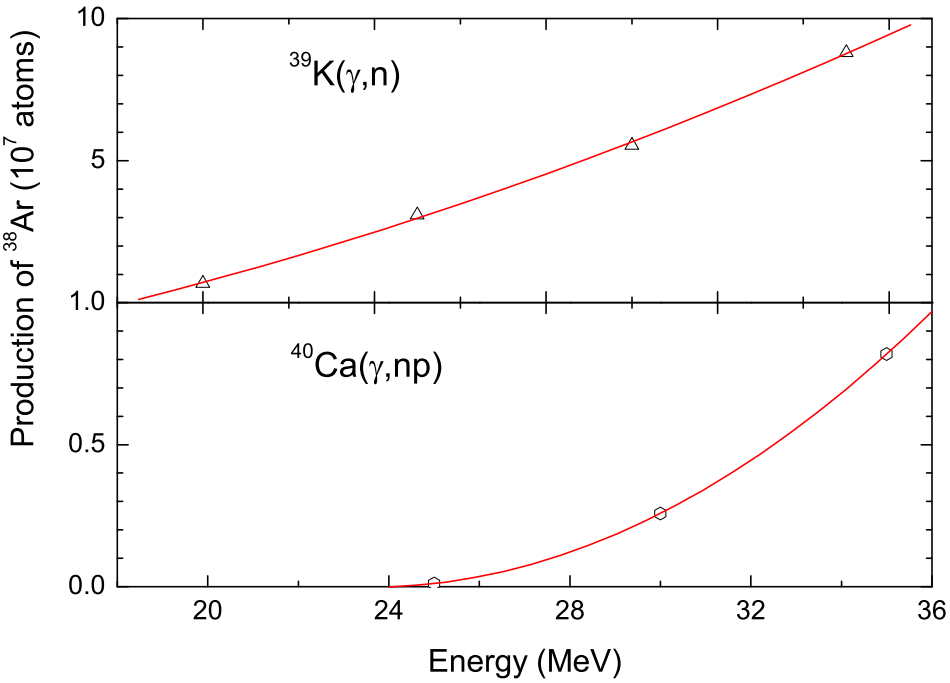

Figure 8: Energy dependence of the amount of ^{38}Ar produced with the $^{39}K(\gamma, n)$ reaction by the FLUKA simulation code. Results for the interfering reaction $^{40}Ca(\gamma, pn)$ are also shown. The solid curves are fits to the data using a quadratic function with the parameters given in the text.

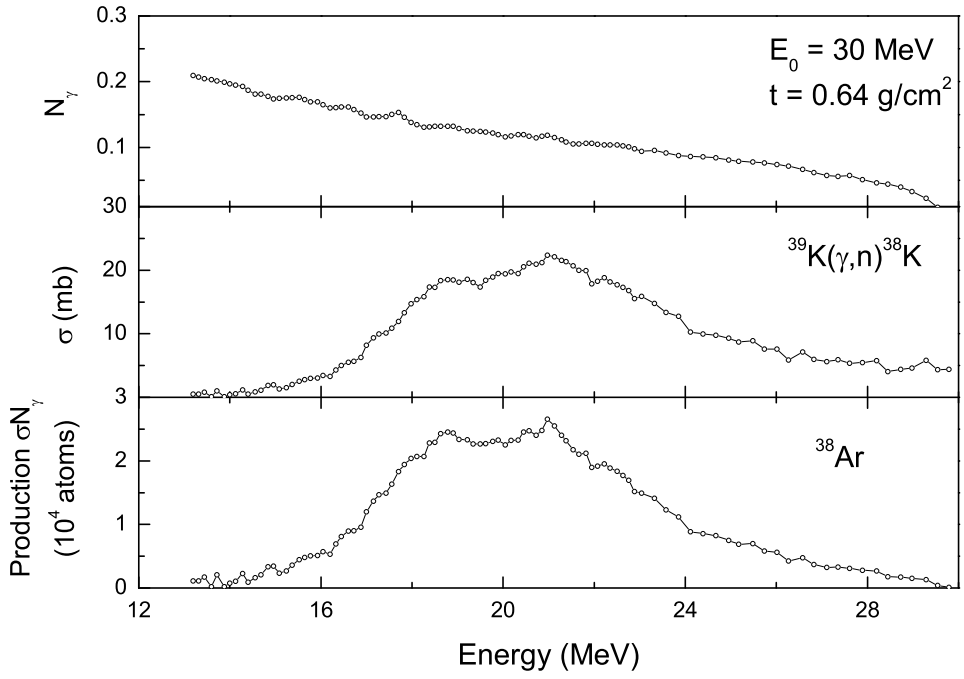

Figure 9: The production value of ^{38}Ar. The upper part shows the photon spectrum obtained by means of the FLUKA simulation.The middle part presents the photoneutron cross section, and the bottom part the ^{38}Ar production rate σN_γ. The results are for the simulation with a 30 MeV electron beam, described in Chapter 3.1.

4 Interfering Reactions

4.1 Prototype Experiment at AERE

A test experiment using the $^{40}Ar/^{38}Ar$ method was carried out already sometime ago at the electron LINAC at Atomic Energy Research Establishment (AERE), Harwell [9]. Two muscovite and two biotite samples of precisely known potassium - argon age were selected for the initial investigation of the feasibility of the method. The samples had high potassium and low calcium contents.

Only four samples could be irradiated simultaneously due to the restrictions of space imposed by the experimental facility available for work. These samples were each packed in a flat "envelope" of aluminium foil, about 0.75×0.75 cm^2, and then the group of samples was arranged to form a cube with a side length of about 1 cm (with aluminium foil wrappings). The sample irradiation was carried out for 130 hours using a 35 MeV electron beam. The samples were placed close to the end of the electron beam tube, behind a gold bremsstrahlung converter plate with a thickness of 0.5 cm. The mean electron beam current was 4 μA. The electrons stopped in the converter plate produced bremsstrahlung photons.

The samples were oriented such that each one should have experienced the same photon flux (neglecting the angular spreading), but there was no space to include monitor materials to measure the flux. The irradiation of these samples was supplementary to a main experiment being carried out on the LINAC at that time and accordingly the duration of the irradiation was

Table 2: Argon isotopic ratios in gamma irradiated micas [9].

Sample	Conventional age (Million years)	Q	$^{40}Ar^*/^{38}Ar$	J
1	18.1	9.65×10^{-3}	64.0 ± 1.9	1.51×10^{-4}
2	81.5	4.42×10^{-2}	296 ± 4	1.49×10^{-4}
3	149	8.22×10^{-2}	564 ± 7	1.46×10^{-4}
4	996	6.96×10^{-1}	4540 ± 40	1.53×10^{-4}

determined by the maximum possible time rather than any quantitative considerations of the received photon flux.

After the irradiation, the samples were transferred to glass ampoules and their argon isotopic ratios were determined using an on-line argon extraction system coupled to an Omegatron mass spectrometer [25].

The results of the analysis are shown in Table 2, where the sample 1 is Bern4M, interlaboratory standard muscovite [26], the sample 2 is P-207, interlaboratory standard muscovite, the sample 3 is biotite - 267 (analytical data provided by Dr. D. C. Rex) and the sample 4 is B3203, MIT interlaboratory standard biotite [27]. From Table 2 one can see, that the mean J value is 1.50×10^{-4}. The results indicate that the method does lead to consistent values for J which would permit the determination of potassium - argon ages of samples, irradiated in this way, with an uncertainty of the order of 2%.

An estimation of J from Eq. (6), using simulation results for the photon yield, was made in the present work in order to check the possibility of quantitative predictions based on FLUKA generated spectra. The obtained value is equal

to 3.1×10^{-4} and agrees well with the data of the experiment, if one considers the various approximations entering into the simulation.

But, as it will be discussed below (see Section 4.3), additional ^{38}Ar from the $^{40}Ca(\gamma, np)$ reaction could be located in the sample which might lead to an overestimation of the age. Thus, the contribution of this background reaction needs to be discussed.

4.2 Overview of Possible Interfering Reactions

In view of the excellent agreement between the values of J obtained from the different samples [9], it seems that any interfering reactions are of negligible importance for the measured probes. In order to assess the potential difficulties which might arise in extending the method to minerals with a less favourable K/Ca ratio, a summary of photon - induced reactions on elements near potassium in the periodic table is given in Table 3 which give rise, ultimately, to isotopes of argon.

Only few precise cross section data exist for photon-induced reactions other than (γ, n). In the light elements (γ, p) reactions occur [28] with a probability comparable with the one for (γ, n), whereas the (γ, α) reaction occurs with considerably smaller probability [18]. The (γ, np) reactions occur at higher energies only.

It becomes clearly from Table 3 that no interaction with isotopes of calcium can give rise to ^{37}Ar or ^{39}Ar (unlike fast reactions on ^{40}Ca which do give rise to ^{37}Ar and thereby provide a method of correction for other interfering isotopes of Ar generated from calcium in the $^{40}Ar/^{39}Ar$ dating method).

An analogous method of correction for such effects would not, therefore, appear to be available in the $^{40}Ar/^{38}Ar$ method. However, ^{39}Ar is produced from the $^{40}K(\gamma,\mathrm{p})$ reaction and because of the relatively long half - life is (in principle) measurable. But, the low natural abundance of ^{40}K limits practical applications.

Table 3: Photon interactions yielding isotopes of argon [9]. P - product isotope with decay scheme(if any). T - threshold energy of photon interaction (MeV). D - decay mode of product isotope with half-life.

Initial	(γ, n)			(γ, p)			(γ, α)			(γ, np)		
isotopes	P	T	D	P	T	D	P	T	D	P	T	D
^{39}K	^{38}K	13.08	β^+	^{38}Ar	6.37					^{37}Ar	18.2	E.C.
(93.08%)	$\downarrow$		7.7 min							$\downarrow$		34 d
	^{38}Ar									^{37}Cl		
^{40}K				^{39}Ar	7.58	β^-	^{36}Cl	6.43	β^+	^{38}Ar	14.16	
(0.012%)				$\downarrow$		265 y	$\downarrow$		3×10^8y			
				^{39}K			^{36}Ar					
^{41}K				^{40}Ar	7.80					^{38}K	17.67	β^-
(6.91%)										$\downarrow$		265 y
										^{38}Ar		
^{40}Ca							^{36}Ar	7.04		^{38}K	21.42	β^-
(96.94%)										$\downarrow$		7.7 min
										^{38}Ar		
^{42}Ca							^{38}Ar	6.23				
(0.64%)												
^{43}Ca							^{39}K	7.58	β^-			
(0.14%)							$\downarrow$		265 y			
							^{39}Ar					
^{44}Ca							^{40}Ar	8.84				
(2.1%)												

4.3 Background Reactions Producing ^{38}Ar

Finally, ^{38}Ar is produced from isotopes other than potassium in the reactions

$$\begin{aligned} {}^{40}Ca \quad & (\gamma, np)^{38}K \xrightarrow{\beta^+} {}^{38}Ar, \\ {}^{42}Ca \quad & (\gamma, \alpha)^{38}Ar, \\ {}^{43}Ca \quad & (\gamma, n\alpha)^{38}Ar. \end{aligned}$$

However, ^{42}Ca and ^{43}Ca have low isotopic abundances of 0.14% and 0.64%, respectively, and in addition can yield ^{38}Ar only in reactions with low cross sections.

The first reaction benefits from the high isotopic abundance of ^{40}Ca (96.9%). The estimates of the amount of ^{38}Ar produced from ^{40}Ca are summarized in Table 4. The results are obtained by means of Eq. (19), where values of σ are taken from [29] and shown in Fig. 10 and the photon spectra were calculated with FLUKA.

As can be seen from the Table 3, the $^{40}Ca(\gamma, np)$ reaction possesses a high threshold energy (21.42 MeV). The yield of ^{38}Ar from ^{40}Ca as a function of the beam energy is also shown in Fig. 8. Finally, the ^{38}Ar production ratio is depicted in Fig. 11. The ratios predicted by the simulations are connected with straight lines to guide the eye. Depending on the $^{38}K/^{40}Ca$ ratio of the probe, one can estimate from Fig. 11 the maximum possible electron energy for an acceptable upper limit of ^{38}Ar resulting from ^{40}Ca - induced reactions.

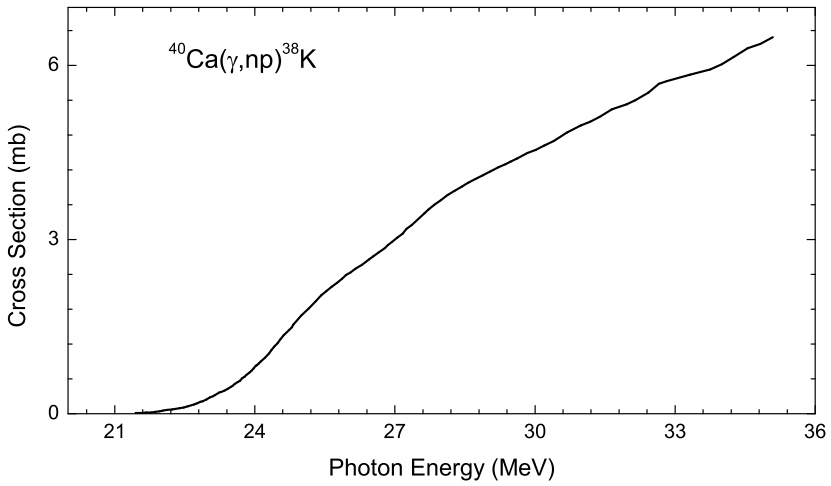

Figure 10: Experimental cross section of the $^{40}Ca(\gamma, np)^{38}K$ reaction [29].

Table 4: ^{38}Ar Yield from ^{40}Ca for different Energies.

Energy (MeV)	σN_γ (mb/s)	^{38}Ar Amount (atoms/s)
20	-	-
25	1388	1.10×10^5
30	31667	2.58×10^6
35	113107	8.19×10^6

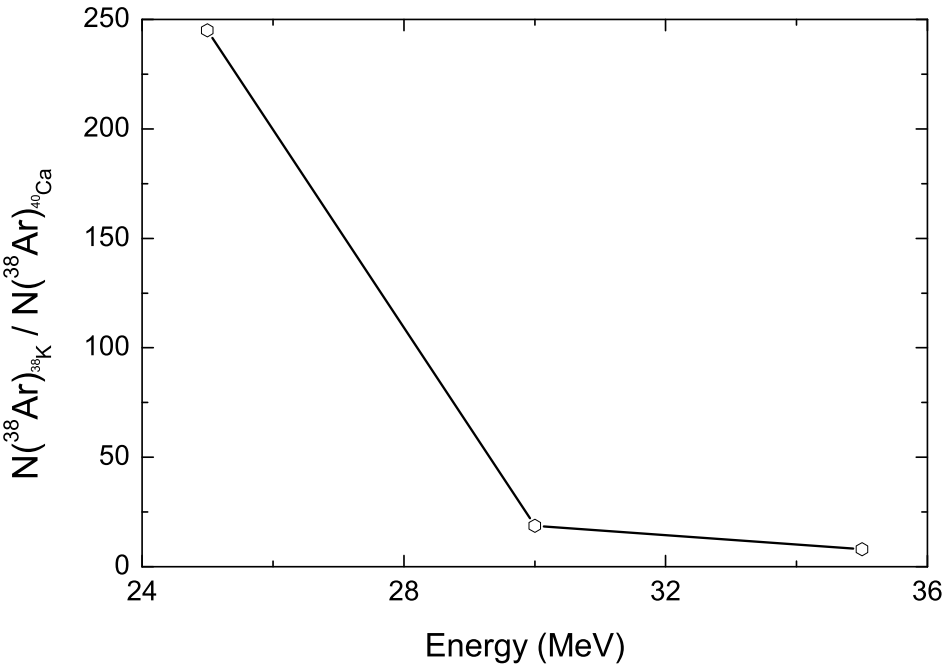

Figure 11: The production ratio of ^{38}Ar from ^{39}K compared with ^{38}Ar produced from ^{40}Ca. The points are connected with straight lines to guide the eye.

5 Possible Experiment at the S-DALINAC

5.1 S-DALINAC

The investigation of the nuclear structure with inelastic electron scattering is one of the most important applications of the Superconducting Darmstadt Linear Electron Accelerator S-DALINAC at the Institute for Nuclear Physics of the Darmstadt University of Technology [30]. Due to its modern concept the S-DALINAC is a high quality source of continuous electron beams with energies up to 130 MeV [31, 32].

The S-DALINAC became the first superconducting continuous-wave linear accelerator of electrons in Europe. Since 1991 the S-DALINAC delivers electron beams with a maximum energy of 130 MeV and currents of up to 60 μA for a wide range of nuclear physics experiments [33]. The layout of the S-DALINAC is shown in Fig. 12.The electron beam can be delivered to several experimental facilities, schematically shown in Fig. 13. The electrons are emitted by a thermionic gun and then accelerated electrostatically to an energy of 250 keV. The required time structure of the electron beam for radio-frequency acceleration in a 3 GHz field is created by a chopper/prebuncher system operating at room temperature. The superconducting injector linac consists of one 2-cell, one 5-cell, and two standard 20-cell niobium cavities cooled to 2 K by liquid helium. The beam leaving the injector has an energy up to 10 MeV and can either be used for radiation physics experiments or for nuclear resonance fluorescence experiments (① in Fig. 13).

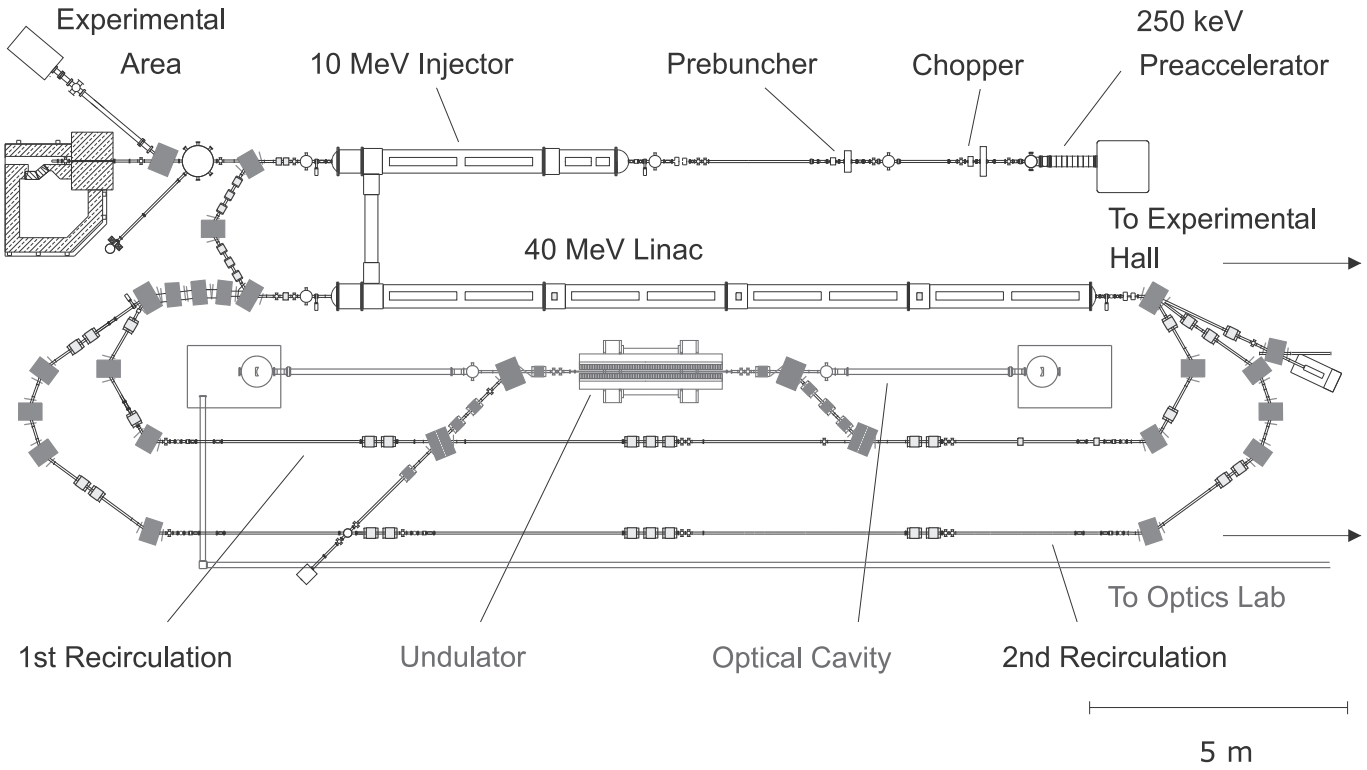

Figure 12: Schematic layout of the S-DALINAC.

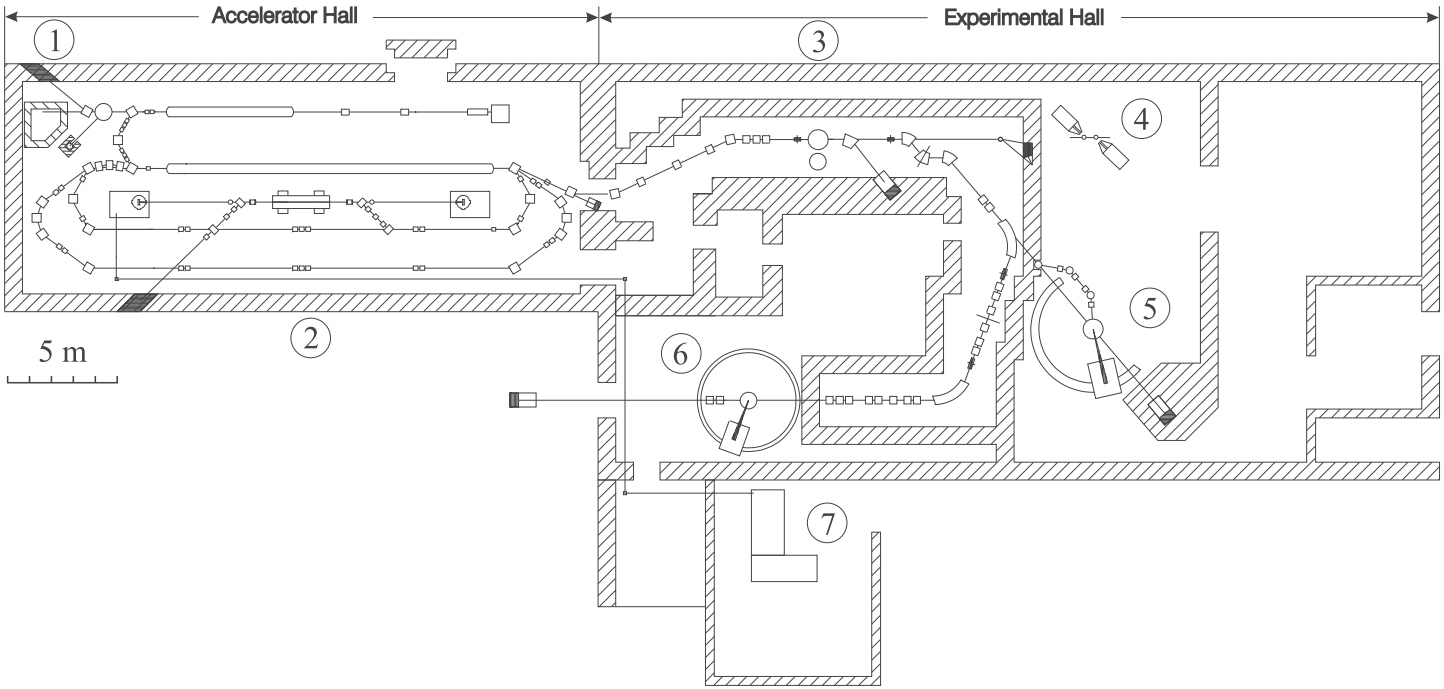

Figure 13: Experimental facilities at the S-DALINAC. ① channeling radiation and (γ, γ') experiments, ② free electron laser, ③ high energy radiation physics, ④ compton scattering off nucleons, ⑤ (e, e') at 180°- and $(e, e'x)$-experiments, ⑥ (e, e')-experiments, ⑦ optic experiments.

Alternatively, it can be bent by 180° and injected into the main accelerator section. This superconducting linac has eight 20-cell cavities which provide an energy gain of up to 40 MeV. After passing through the main linac the electron beam may be extracted towards the experimental hall or it can be recirculated and reinjected one or two times into the main linac using two separated recirculating beam transport systems. Additionally, in the first recirculation beam-line an infrared Free Electron Laser (FEL) is located (② in Fig. 13).

A wide range of electron scattering experiments is carried out using the QCLAM spectrometer (⑤ in Fig. 13) and a high resolution facility with a magic-angle spectrometer (⑥ in Fig. 13). The QCLAM spectrometer has a large angular and momentum acceptance and is used for (e,e′x)-coincidence and for (e,e′)-experiments at 180°. The magic-angle spectrometer operates in the so-called "energy-loss" mode that enables to perform high resolution (e,e′)-experiments independently of the energy spread of the electron beam.

5.2 Experimental Setup

Figure 14 shows a setup for bremsstrahlung experiments behind the main accelerator of the S-DALINAC. It is constructed [34] for experiments with high-energy electrons ($E_0 = 50 - 100\ MeV$). A 0.3 mm thick gold plate (0.1 radiation length) with a diameter of 2 mm is used as radiator. This target (④ in Fig. 14) is placed in a special tube, which provides good thermal contact of the target with the environment for effective cooling.

Behind the radiator the scattered electron beam is deflected by about

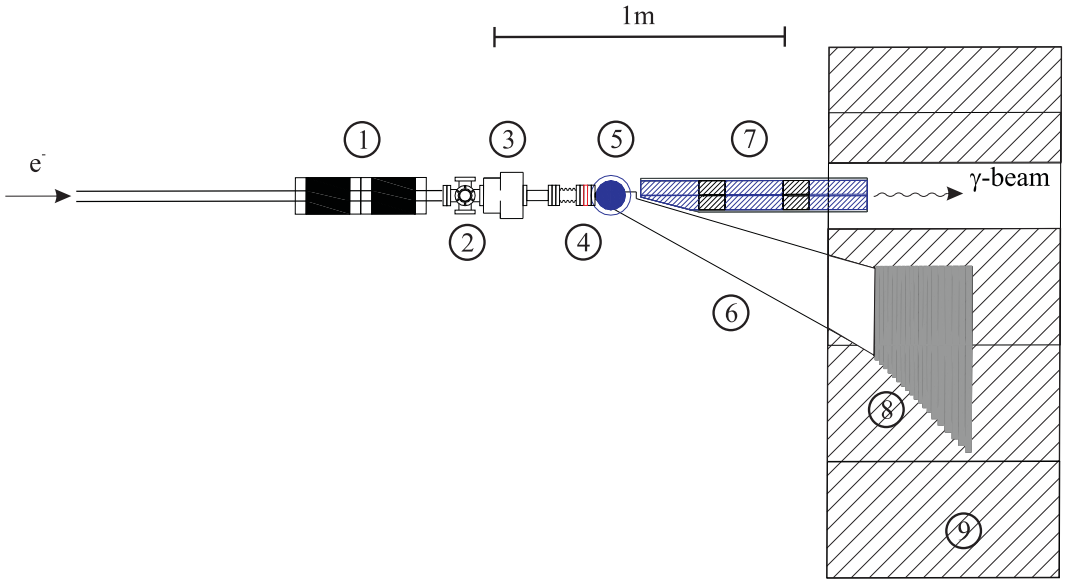

Figure 14: Experimental Setup. ① steering magnets, ② OTR-Al-Oxid target, ③ beam position/current monitor, ④ converter target, ⑤ cleaning magnet, ⑥ vacuum tube, ⑦ collimator system, ⑧ beam dump, ⑨ concrete wall.

23° from the original axis by means of a compact dipole magnet (⑤ in Fig. 14). Since the edge field from the dipole magnet at the position of the bremsstrahlung target is not negligible, the target is additionally protected with a magnet-field shielding made from soft iron. The electron beam is broadening during interaction with the radiator, therefore the poles of the dipole magnet are not parallel, but have an opening angle of 16°.

The precise position of the electron beam - at this place 1 mm in diameter - can be controlled online by steering magnets (① in Fig. 14) with the help of a position-sensitive high frequency monitor system (③ in Fig. 14) and an optical transition radiation (OTR) target (② in Fig. 14).

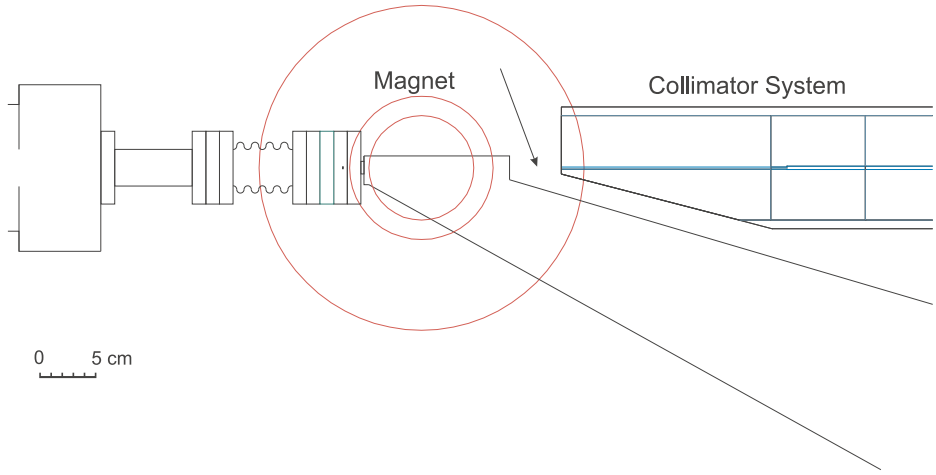

Figure 15: Details of the experimental setup . The arrow shows the free available space for the probe between the dipole magnet and the collimator.

The air cooled beam dump (⑧ in Fig. 14), composed of aluminium and lead, is placed in the wall of the concrete shielding and allows to monitor the beam current. The bump is constructed to allow for a heat load up to 1.5 kW.

Behind the dipole magnet the Bremsstrahlung cone will be collimated into a 10×20 mm^2 photon beam. The collimator (⑦ in Fig. 14) is 20 cm long and it consists of several layers of lead with different slit parameters and some additional layers of polyethylene for shielding fast neutrons produced in the collimator. It is designed for a study of Compton scattering of the proton using a novel high - pressure hydrogen chamber as active target [34].

A maximum photon flux is necessary for the present experiment, so the

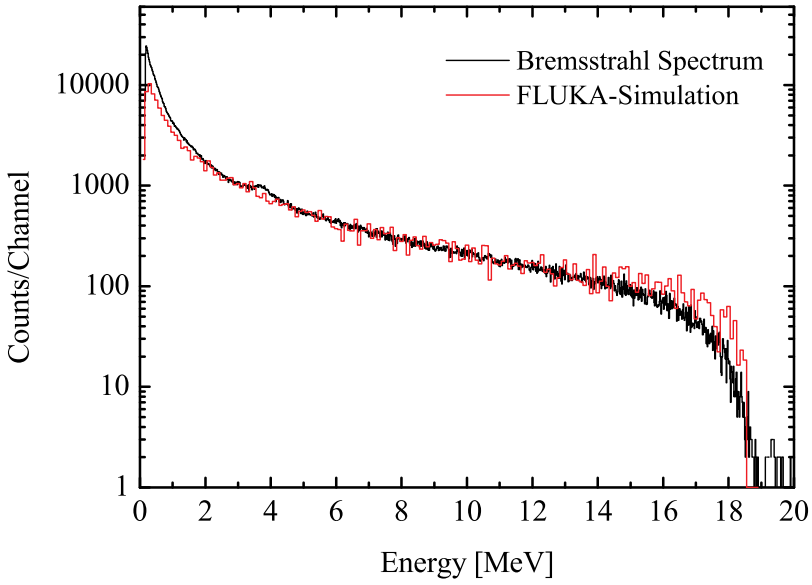

Figure 16: The low energy spectrum at 19.5 MeV and FLUKA simulation for 19 MeV [34].

probe should be situated as close to the target as possible in the free space between the dipole magnet ⑤ and the collimator ⑦ . This region is shown in details in Fig. 15. The available space in the area indicated by the arrow is equal to 5 cm.

In this area behind the collimator a measurement of the bremsstrahlung spectrum at 19.5 MeV was performed. In Fig. 16 one can see the good agreement between the experimental spectrum and the spectrum obtained from the simulation when trying to incorporate the geometry of the measurement [34].

5.3 The Probe

The samples will be placed in a 5 cm long quartz ampoule, which has a diameter of about 0.6 cm. The samples have a typical weight between 10 and 50 mg. Each sample is wrapped in about 40 mg Al foil. So, each sample is an Al-pellet approximately 1-3 mm thick and 4 mm in diameter. In total 10 samples (total weight of about 500-900 mg) are used: one Ca, one Cl and one K monitor, at least three age standards that also monitor the flux variation, and 4-5 samples to be investigated. So, about 3 cm of the quartz ampoule are filled with samples, the remaining 2-3 cm are empty because one needs some distance between them when the ampoule is sealed.

6 Conclusion

An investigation of the feasibility of $^{39}K(\gamma, n)$ experiments for mineral age determination at the S-DALINAC has been carried out. It was demonstrated that qualitative predictions for ^{38}Ar production and Ar isotope ratios are possible with the help of modern methods (for example, a Monte Carlo simulation for the photon flux). The quantitative accuracy is limited to a factor of about two because of simplifications made in the simulation geometry.

A limitation of the available setup at the S-DALINAC is caused by the relatively thin bremsstrahlung target. The thickness can not be easily increased because the dipole magnet and Faraday cup systems were not designed for thick target experiments. Furthermore, a setup for thick target bremsstrahlung would require major investments, because heavy shielding would be needed. Also the problem of induced activity appears.

Experiments seem feasible on time scales of hours to a few days for not too small K/Ca ratios. Exact limits must be determined experimentally in a test run, planned for 2003.

References

[1] G. Faure, *Principles of Isotope Geology*, (John Wiley and Sons, New York, 1986) 66.

[2] G.B. Dalrymple and M.A. Lanphere, *Potassium-Argon Dating*, (W.H. Freeman, San Francisco, 1969).

[3] R.B. Firestone, Table of Isotopes, (John Wiley and Sons, New York, 1996).

[4] I. McDougall, T.M. Harrison, *Geochronology and Thermochronology by the* $^{40}Ar/^{39}Ar$ *method*, (Oxford Univ. Press, New York, 1988).

[5] C.M. Merrihue and G.Terrihue, J. Geophys. Res. **71** (1966) 2852.

[6] N.R. Brereton, Earth Planet. Sci. Letters **8** (1970) 39.

[7] G.N. Berger, D.York, Earth Planet. Sci. Letters **10** (1971) 227.

[8] J.G. Mitchell, Geochim. Cosmochim. Acta **32** (1968) 781.

[9] J.G. Mitchell, Earth Planet. Sci. Letters **14** (1972) 91.

[10] R.J. Howerton, D. Braff, W.J. Cahill and N. Chazan, UCRL Report **14006** (1964).

[11] A. Veyssiere, H. Beil, R. Bergere, P. Carlos and A. Lepretre, Nucl. Phys. **A159** (1970) 561.

[12] O.V. Bogdankevich, *Methods in Bremsstrahlung Research*, (Academic Press, London, 1966).

[13] W.R. Leo, *Techniques for Nuclear and Particle Physics Experiments*, (Springer, Berlin-Heidelberg, 1994).

[14] Review of Particle Properties, Phys. Rev. **D45**, Part II (1992).

[15] H.A. Bethe and L.C. Maximon, Phys. Rev. **93** (1954) 768.

[16] L.I. Schiff, Phys. Rev. **83** (1951) 252.

[17] Program FLUKA, http://pcfluka.mi.infn.it/.

[18] A.E.S. Green, *Nuclear Physics*, (McGraw Hill, London, 1955) 469.

[19] B.L. Berman and S.C. Fultz, Rev. Mod. Phys. **47** (1975) 713.

[20] C.Tzara, C.R. Acad. Sci. **56** (1957) 245.

[21] L.W. Jones and K.M. Terwilliger, Phys. Rev. **91** (1953) 659.

[22] M. Goldhaber and E. Teller, Phys. Rev. **74** (1948) 1046.

[23] H. Steinwedel and J.H.D. Jensen, Naturforsch. **A5** (1950) 413.

[24] M. Trieloff, private communication.

[25] R.L. Grasty and J.A. Miller, Nature **207** (1965) 1146.

[26] E. Jager, E. Niggli and H. Baethge, Schweiz. Mineral. Petrog. Mitt. **43** (1963) 465.

[27] M.A. Lanphere and G.B. Dalrymple, J. Geophys. Res. **70** (1965) 3947.

[28] E. Hayward, Photonuclear Reactions, in: *Nuclear Structure and Electromagnetic Interactions* (Oliver and Boyd, Edinburgh, 1965) 164.

[29] E. Bramanis, Nucl. Phys. **A175** (1971) 17.

[30] A. Richter, *Proc. 5th Europ. Part. Acc. Conf.*, ed. S. Meyer et al., (IOP Publishing, Bristol, 1996) 110.

[31] A. Richter, Prog. Part. Nucl. Phys. **44** (2000) 3.

[32] S. Strauch, P. von Neumann-Cosel, C. Rangacharyulu, A. Richter, G. Schrieder, K. Schweda and J. Wambach, Phys. Rev. Lett. **85** (2000) 2913.

[33] P. von Neumann-Cosel, F. Neumeyer, S. Nishizaki, V.Yu. Ponomarev, C. Rangacharyulu, B. Reitz, A. Richter, G. Schrieder, D.I. Sober, T. Waindzoch and J. Wambach, Phys. Rev. Lett. **82** (1999) 1105.

[34] S. Watzlawik, Dissertation, TU Darmstadt, in preparation.

Acknowledgements

At this place I would like to thank all the persons who have contributed to the success of this work.

On the first place I would like to sincerely thank *Professor Dr. Dr. h. c. mult. Achim Richter* for the given opportunity to work on such an exciting topic under his supervision and to sense the climate of constructive team work in the modern scientific laboratory. Without you this work would not be imaginable.

Further on I would like to thank *Privatdozent Dr. Peter von Neumann-Cosel* for the numerous useful discussions during the realization of this diploma thesis and for valuable remarks that he has made during the reading of this thesis and the significance of which it is difficult to overestimate.

I address my heartfelt gratitude to *Dr. Harald Genz* for his every day help, care and support.

I would like to express my gratitude also to *Oleksiy Burda, Natalya Ryezaeyva, Artem Shevchenko, Dr. Sergiy Khodyachykh* and *Yaroslav Kalmykov* for their support and numerous significant advices. Thank you very much!

I am grateful to *Dipl.-Phys. Steffen Watzlawik* for all given information and his help during my work.

I would like to express my gratitude to *V.D. Afanas'ev, E.S. Shmatko, A.F. Shchus* and Chair of the Experimental Nuclear Physics of the Karazin Kharkiv National University (Ukraine) for the time they have spent for my education.

Finally, my heartful gratitude to my family and to my friends in Ukraine. Your thoughts and your care were supporting me very much during my study in the Karazin Kharkov University and during my stay in Darmstadt.